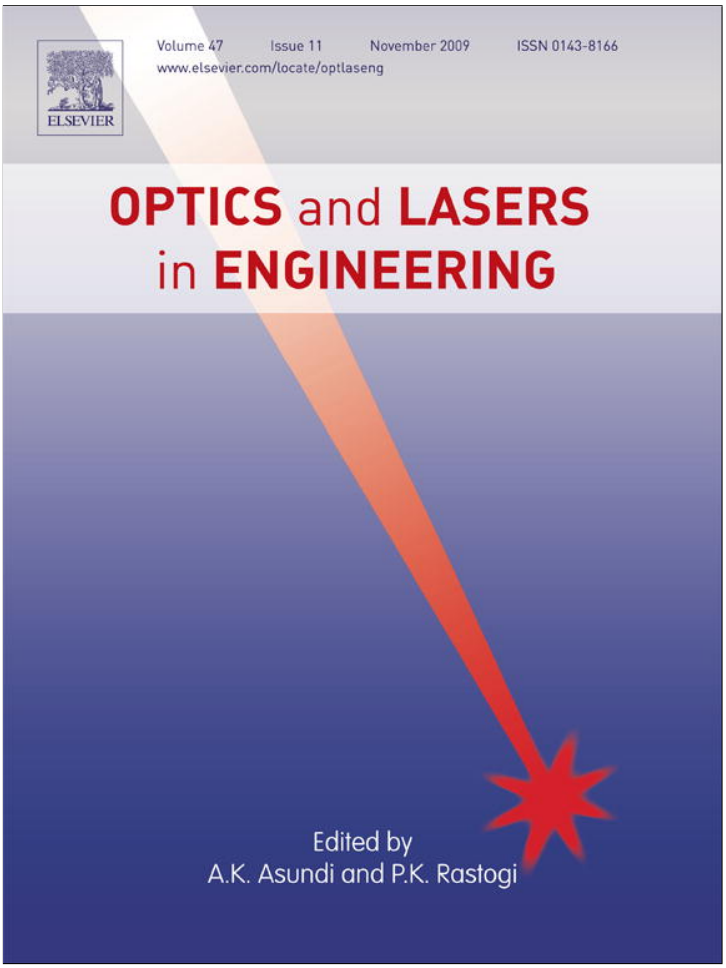

Optics and Lasers in Engineering 47 (2009) 1189–1194

Contents lists available at ScienceDirect

Optics and Lasers in Engineering

journal homepage: www.elsevier.com/locate/optlaseng

Modified smart pixel mapping method for displaying orthoscopic 3D images in integral imaging

Dong-Hak Shin [a,*], Byung-Gook Lee [a], Eun-Soo Kim [b]

[a] Department of Visual Contents, Dongseo University, San 69-1, Jurye-2-Dong, Sasang-Gu, Busan 617-716, Republic of Korea
[b] 3DRC, Department of Electroni Engineering, Kwangwoon University, 447-1 Wolge-Dong, Nowon-Go, Seoul 139-701, Republic of Korea

ARTICLE INFO

Article history:
Received 23 September 2008
Received in revised form
9 June 2009
Accepted 10 June 2009
Available online 15 July 2009

Keywords:
3D display
Integral imaging
Orthoscopic image
Elemental images
Depth conversion

ABSTRACT

In this paper, we propose a modified smart pixel mapping (MSPM) method for displaying orthoscopic three-dimensional (3D) images with a function of depth control in integral imaging system. In the proposed MSPM, the depth-converted elemental image array (EIA) is obtained through the pixel mapping process and the image interpolation technique. The proposed method gives us the depth conversion at distances different from the position of 3D object and provides various types of EIAs using only an original EIA for orthoscopic images. To show the usefulness of the proposed method, we carry out the preliminary experiments and present the experimental results.

1. Introduction

The advent of integral imaging technology can be traced back to 1908, which was first proposed by Lippmann [1]. Since then, integral imaging has been gaining great attention among researchers as it is a promising three-dimensional (3D) technology which is able to deliver autostereoscopic, continuous viewing points, full parallax, and full color view to the observers [2–6]. With integral imaging technology, observers do not need to wear special glasses to perceive the 3D effect.

A general integral imaging system as shown in Fig. 1 consists of two processes: pickup and reconstruction. In the pickup process, a lenslet array is used to capture the 3D object. Each of the lenslets provides different perspective views of the 3D object, which results in a collection of demagnified 2D images, known as an elemental image array (EIA). To record the EIA, a 2D image sensor such as a charge coupled device (CCD) sensor is used. In order to reconstruct the 3D image, rays are reversely propagated through the EIA and a similar lenslet array is used in the pickup process.

In the integral imaging reconstruction, the reconstructed 3D image is in pseudoscopic form, which is reverse in depth. Therefore, the additional procedures are needed to convert the 3D image from pseudoscopic to orthoscopic form [7–13]. Most of these methods might degrade the image quality of the 3D image after the conversion process due to the use of optical devices [9,11]. To overcome these problems, a computational reconstruction method called smart pixel mapping (SPM) was reported [12]. SPM is a computational depth-reverse process based on the concept of facetted structure of reconstruction [14] and provides real, undistorted and orthoscopic integral images. However, the computational structure for SPM is very limited to the fixed distance between the lenslet array and the virtual pinhole array.

In this paper, we propose an improved digital pixel mapping method, which is called modified SPM (MSPM). In contrast to the conventional SPM method, the proposed MSPM can control the position of the virtual pinhole array for the depth-converted EIA during the mapping process. The original EIA is digitally mapped to an output plane to form a depth-converted EIA, which can provide orthoscopic images of 3D objects.

2. Review of SPM

The principle of the conventional SPM method is illustrated in Fig. 2. SPM is a computational depth-reverse process in which the original EIA is convertible to ones recorded at the different virtual pickup distance [12].

The depth conversion in SPM involves a two-step recording process. In the first step as shown in Fig. 2(a), the 3D object is assumed to be located at a distance without braiding effect [15] and recorded as the first (original) EIA. In the second step shown in Fig. 2(b), a 3D image is reconstructed by using the original EIA at the distance as it was captured. The reconstructed 3D image is

* Corresponding author.
E-mail address: shindh2@dongseo.ac.kr (D.-H. Shin).

0143-8166/$ - see front matter © 2009 Elsevier Ltd. All rights reserved.
doi:10.1016/j.optlaseng.2009.06.004

then recorded again by a virtual pickup system with virtual pinhole array to produce depth-converted EIA. Here SPM is implemented using a direct pixel mapping process by using the original EIA denoted by E. The conversion process is done digitally to produce the second set of depth-converted EIA denoted by T. The SPM algorithm for 1D case is formulated as

$$T_m^n = E_k^l, \tag{1}$$

where

$$l = (M+1) - n, \tag{2}$$

and

$$k = \begin{cases} m + M/2 - n & \text{if } M \text{ is even} \\ m + (M+1)/2 - n & \text{if } M \text{ is odd} \end{cases}. \tag{3}$$

In Eq. (1), T is the output of E after applying the SPM. The subscripts m and k correspond to the elemental image number and n and l are the pixel numbers in the given elemental image, respectively. The values M and N are the total number of elemental images and the total pixels per elemental image, respectively. We set T equal to zero if the corresponding $k<1$ or $k>M$. The effective distance of SPM is given as

$$d = N \times g, \tag{4}$$

where g is the focal length of lenslet array. In general, the SPM process is limited to d regardless of the distance of 3D objects.

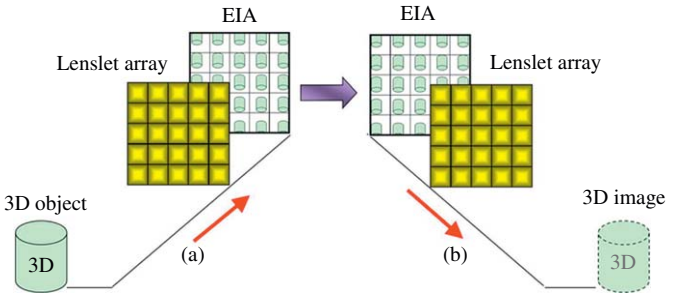

Fig. 1. A general integral imaging system: (a) pickup and (b) reconstruction.

3. Proposed MSPM method

In this paper, we proposed a digital pixel mapping method to improve the performance by controlling the effective distance of SPM. The proposed method gives us the depth conversion at distances different from the position of 3D object and provides various types of EIA using only original EIA for orthoscopic images. The depth-converted EIA is obtained through the pixel mapping process and the image interpolation technique.

3.1. Pixel mapping process

To explain the procedure of the proposed method, let us consider one-dimensional pixel mapping between lenslet array and virtual pinhole array shown in Fig. 3. To understand the function of depth control of the proposed method, we show two examples when the different distances are used. Fig. 3(a) shows the same case with the original SPM. On the other hand, the case when using the different distance is shown in Fig. 3(b). This method is called modified SPM. The extension to 2D case is straight forward. As shown in Fig. 3, let us consider an input plane L and an output plane R. The parameter z is the mapping distance between two arrays in the L-plane and the R-plane. Considering the symmetry between two arrays, the distance z is calculated by $z = d/n$ where d is the effective distance of the conventional SPM and n is an integer number.

First, we define the relationship between lenslet in L-plane and pinhole in R-plane by measuring the angles θ_{ij}, which is

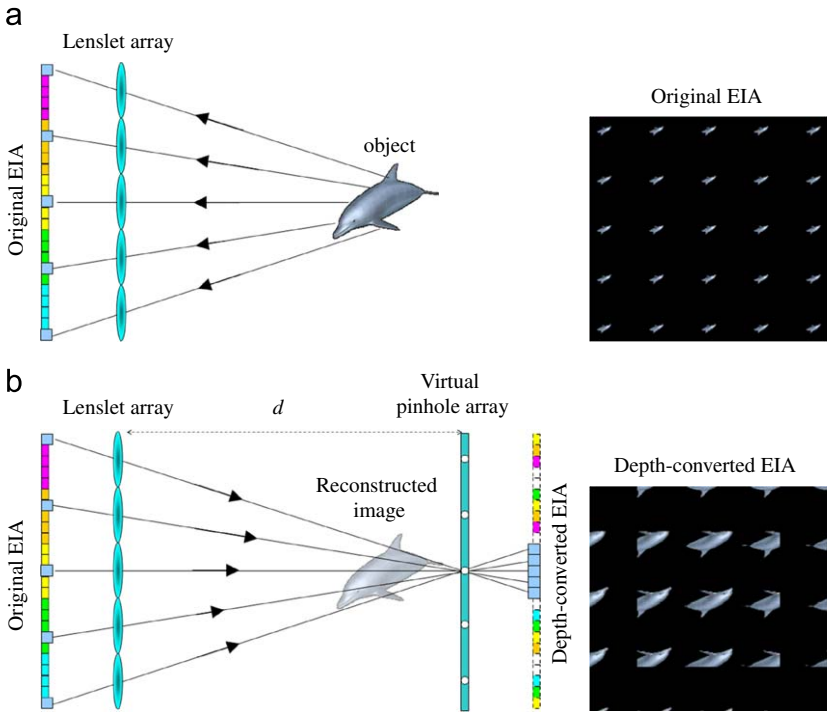

Fig. 2. Principle of the conventional SPM method: (a) pickup of original EIA and (b) pickup of depth-converted EIA.

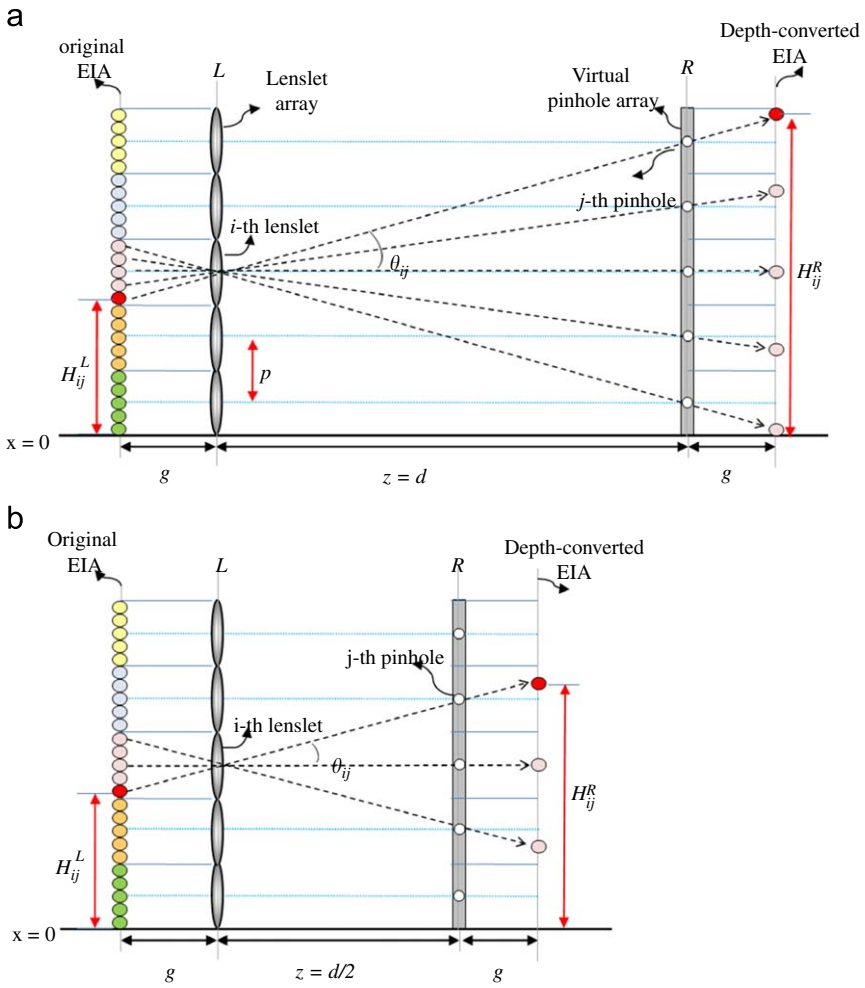

Fig. 3. Ray mapping of the proposed MSPM method: (a) when $z = d$ and (b) when $z = d/2$.

given by

$$\tan\theta_{ij} = \frac{(i-j)p}{z}, \tag{5}$$

the subscripts i and j indicate i-th and j-th elemental image in each image plane, respectively, and p is the size of the single lenslet.

After calculating the θ_{ij}, the next step is to find the mapping pixel in L-plane and then mapping into the corresponding pixel in R-plane. From Fig. 3, the height of the mapping pixel and its corresponding pixel are calculated as

$$H_{ij}^L = (i-1/2)p + g\tan\theta_{ij}, \tag{6}$$

and

$$H_{ij}^R = (j-1/2)p - g\tan\theta_{ij}, \tag{7}$$

respectively. From Eqs. (6) and (7), we can easily perform the pixel mapping between the lenslet array and the virtual pinhole array as shown in Fig. 3. Here, we can see that the MSPM can be easily configured to obtain the same result as produced by SPM by setting the mapping distance equal to $z = pg$. By satisfying this constraint, EIA produced by MSPM is exactly the same as those produced by using SPM.

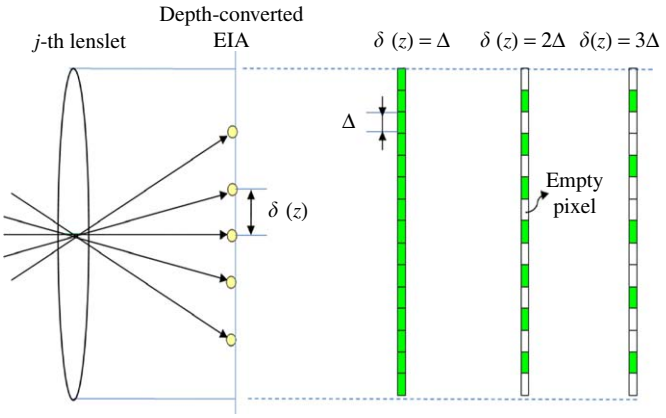

Fig. 4. Explanation of the presence of empty pixels in the depth-converted EIA.

3.2. Image interpolation for empty pixels

After finishing the pixel mapping based on Eqs. (6) and (7), we might not obtain the final depth-converted EIA due to the existence of empty pixels in the R-plane. The empty pixels mean that the pixel value is not allowed because there is no mapping relation from the pixels in the L-plane. Fig. 4 explains why the empty pixels happen in the depth-converted EIA. Consider rays

coming through the j-th pinhole in the L-plane. The rays are uniformly mapped into the depth-converted EIA since all the pinhole distances are the same. The mapping interval, denoted by $\delta(z) = gp/z$, is a function of z. δ increases as z decreases. As shown in Fig. 4, if the single pixel size of the depth-converted EIA is Δ, we can consider several cases of different z values. When $\delta(z) = \Delta$ all the pixels are filled with a certain intensity value. This case is the identical condition of the conventional SPM. However, the sampling mismatching exists in the L-plane when $\delta(z)$ is not equal to Δ. In this case, the empty pixels appear as shown in the right of Fig. 4. Thus, to obtain the final depth-converted EIA, the empty pixels should be interpolated as a new intensity value. To do so, we apply the interpolation technique to the EIA with empty pixels. Fig. 5 shows the concept of using an interpolation technique in the EIA with empty pixels. The interpolation technique can interpolate new pixels among four neighboring pixels in the EIA. Here, various popular interpolation techniques such as the standard linear interpolation and the cubic convolution interpolation are used to interpolate new pixel values [16–18]. An example using the standard linear interpolation is shown in Fig. 5. The average value is inserted as the new pixel value considering the distance rate between neighboring pixels. In this paper, a popular linear interpolation technique is used for demonstrating our proposed method. Let $f(x_k)$ be the sampled version of a continuous function $f(x)$. The relationship between $f(x)$ and its samples $f(x_k)$ is represented in the form

$$f(x) = \sum_{k=0}^{N-1} f(x_k)\beta(x-k), \tag{8}$$

where $\beta(x)$ is the linear interpolation kernel, which is defined as

$$\beta_1(x) = \begin{cases} 1-|x|, & 0 \le |x| < 1 \\ 0, & \text{elsewhere.} \end{cases} \tag{9}$$

After all empty pixels are filled with new intermediate values using the linear interpolation technique, the final depth-converted EIA for the proposed method is obtained.

4. Experiment and results

To show the effectiveness of the proposed MSPM method, computational experiments on the reconstruction of two test images were performed. The experimental structure is shown in Fig. 6. The lenslet array used in this experimental setup is composed of 32×32 lenslets. The interval between lenslets is $p = 1.024$ mm and the gap g between the elemental images and the lenslet array is 3 mm. Two color character images 'D' and 'S' shown in Fig. 6 are used as test images. Each of the patterns has 1024×1024 pixels. Red 'D' image is located at 32 mm from the lenslet array and green 'S' image is 64 mm.

In the experiment structure shown in Fig. 5, we first synthesize the EIA by the computational pickup based on simple ray geometry [6]. The resultant EIA is shown in Fig. 7(a). Next, the synthesized EIA was modified using the proposed MSPM method in order to obtain a depth-converted EIA.

For the demonstration of our MSPM method, we performed the depth-conversion experiments using the original EIA. The first experiment is the case when $z = 96$ mm where the condition is

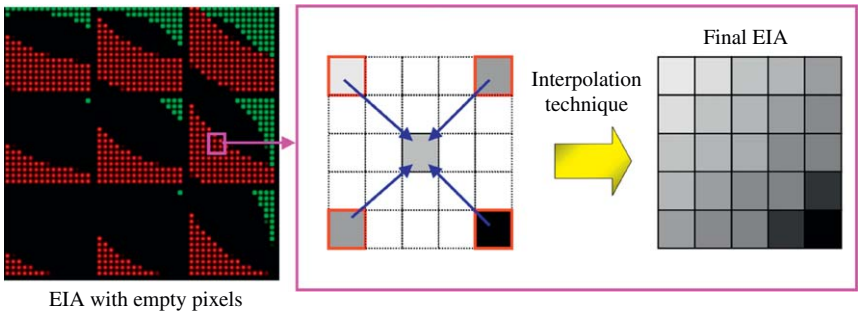

Fig. 5. Interpolation for EIA with empty pixels.

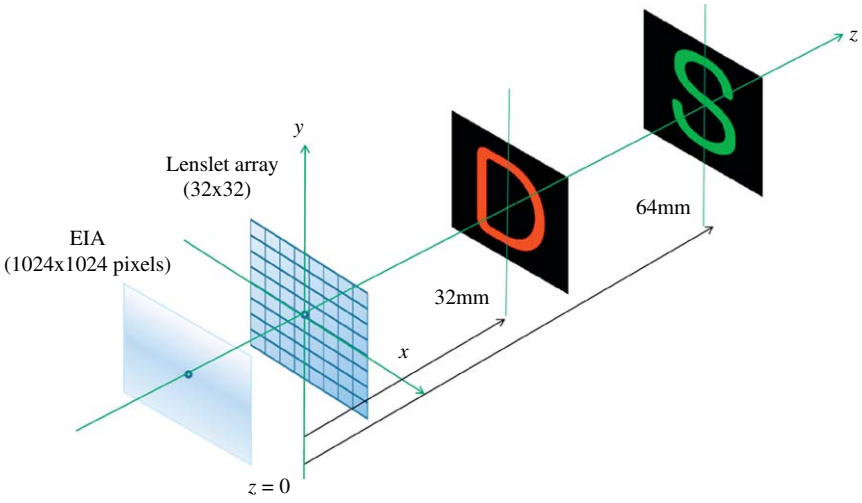

Fig. 6. Experimental setup for the pickup of EIA.

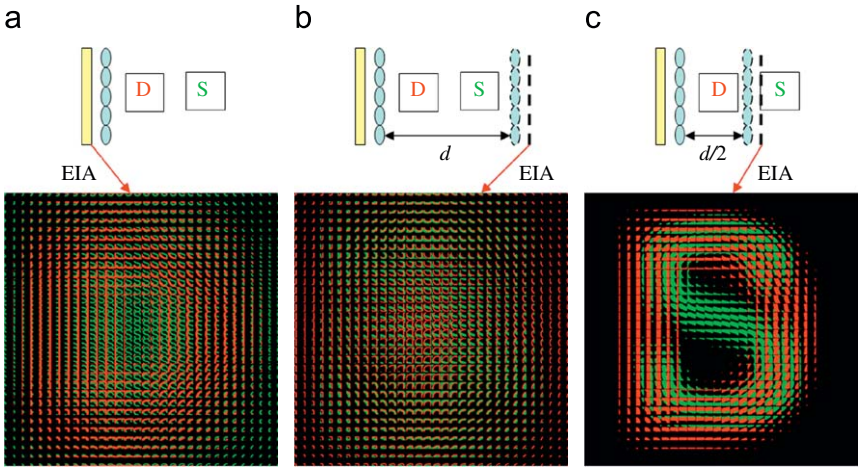

Fig. 7. (a) Original EIA, (b) depth-converted EIA at $z = 96$ mm and (c) depth-converted EIA at $z = 48$ mm.

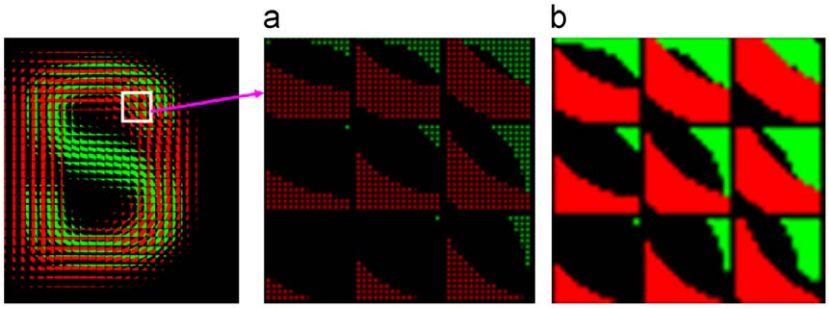

Fig. 8. Example of interpolation process in EIA with empty pixels.

the same with that of the conventional SPM. Using the MSPM process of Fig. 3, the depth-converted EIA was obtained and it is shown in Fig. 7(b). In this case, we obtained the EIA without an additional interpolation technique due to the full pixel mapping between the original EIA and the depth-converted EIA. On the other hand, the second one is the case when $z = 48$ mm where the distance of virtual pinhole array is located between two character images. In this case, we can obtain the EIA pickuped through both real and virtual image planes. However, the depth-converted EIA has many empty pixels because of pixel sampling with the interval of every two pixels according to Eqs. (6) and (7). Fig. 8 shows an example of some enlarged elemental images from the EIA with empty pixels. As shown in Fig. 8(a), the EIA has discrete pixels. Thus, we applied the linear interpolation technique to the EIA. The final EIA is shown in Fig. 8(b). It can be seen that all empty pixels were interpolated with proper values. After an interpolation process, the finally depth-converted EIA was obtained as shown in Fig. 7(c).

To evaluate the characteristics of three EIAs shown in Fig. 7, we have simulated the reconstruction stage. In the reconstruction process, the observer is at a distance 500 mm from the lenslet array and sees the reconstructed images through the lenslet array. For three EIAs of Fig. 8, we calculated the reconstructed images, respectively. They are shown in Fig. 9, respectively. Here, we simulated a lateral displacement for the observer from $x = -64$ mm to $x = +64$ mm. The position $x = 0$ is the case where the observer is centered at the optical axis of the central lenslet. To make them easy to understand, we added each image formation in the left of Fig. 9. Fig. 9(a) shows the pseudoscopic images reconstructed from the original EIA without any modification. The 'D' image is behind 'S' image due to the pseudoscopic reconstruction. On the other hand, Fig. 9(b) and (c)

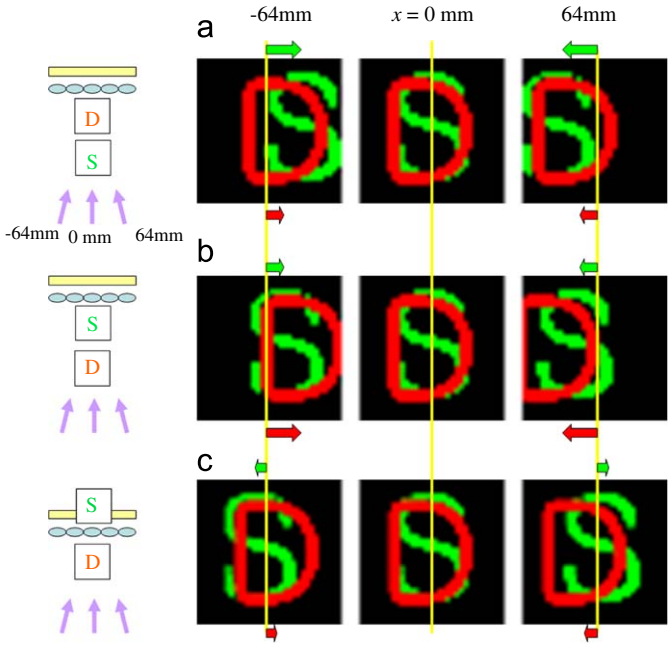

Fig. 9. Computationally observed images: (a) with original EIA, (b) with depth-converted EIA at $z = 96$ mm and (c) with depth-converted EIA at $z = 48$ mm.

shows the orthoscopic images reconstructed from the depth-converted EIA using the proposed MSPM method. Because the 'D' image is in front of 'S' image, we obtained orthoscopic images. In particular, our method allows the orthoscopic reconstruction in both real and virtual image fields using selected virtual pinhole

array at the intermediate position of two objects as shown in Fig. 9(c). From the results of Fig. 9, we can see that the MSPM is generated to various types of EIA.

5. Conclusion

Even though the proposed method was successfully demonstrated, the interpolation technique can largely be dependent on the complexity of 3D object for the practical application. That is, it can provide a good performance for the simple 3D object because of good prediction from an interpolation technique. For the complex 3D object, however, it is not easy to interpolate the exact pixels without more information of 3D object. This will be one of our future works.

In conclusion, a digital pixel mapping method for displaying orthoscopic 3D images in the integral imaging system was proposed. In the proposed method, the depth-converted EIA was obtained through the pixel mapping process and the image interpolation technique. Since the proposed method can provide the depth conversion at distances different from the position of 3D object and various types of EIA using only original EIA for orthoscopic images, it is considered as an improved version of the conventional smart pixel mapping. To prove our statement, we have performed the experiments and the results have been presented. We expect that the proposed method can be usefully applied to the practical integral imaging system.

Acknowledgment

This research was supported by the MKE (Ministry of Knowledge Economy), Korea, under the ITRC (Information Technology Research Center) support program supervised by the IITA (Institute of Information Technology Assessment) (IITA-2009-C1090-0902-0018).

References

[1] Lippmann G. La photographic intergrale. C R Acad Sci 1908;146:446–51.
[2] Stern A, Javidi B. Three-dimensional image sensing, visualization and processing using integral imaging. Proc IEEE 2006;94:591–607.
[3] Okano F, Hoshino H, Arai J, Yuyama I. Real-time pickup method for a three-dimensional image based on integral photography. Appl Opt 1997;36:1598–1603.
[4] Jang J-S, Javidi B. Improved viewing resolution of three-dimensional integral imaging by use of nonstationary micro-optics. Opt Lett 2002;27:324–326.
[5] Lee B, Jung S, Park J-H. Viewing-angle-enhanced integral imaging by lens switching. Opt Lett 2002;27:818–20.
[6] Shin D-H, Lee B, Kim E-S. Multidirectional curved integral imaging with large depth by additional use of a large-aperture lens. Appl Opt 2006;45:7375–7381.
[7] Okano F, Hoshino H, Arai J, Yuyama I. Real-time pickup method for a three-dimensional image based on integral photography. Appl Opt 1997;36:1598–1603.
[8] Park J-H, Min S-W, Jung S, Lee B. Analysis of viewing parameters for two display methods based on integral photography. Appl Opt 2001;40:5217–5232.
[9] Jang J-S, Javidi B. Two-step integral imaging for orthoscopic three-dimensional imaging with improved viewing resolution. Opt Eng 2002;41:2568–71.
[10] Jang J-S, Javidi B. Three-dimensional projection integral imaging using micro-convex-mirror arrays. Opt Express 2004;12:1077–83.
[11] Jang J-S, Javidi B. Formation of orthoscopic three-dimensional real images in direct pickup one-step integral imaging. Opt Eng 2003;42:1869–70.
[12] Martinez-Corral M, Javidi B, Martínez-Cuenca R, Saavedra G. Formation of real, orthoscopic integral images by smart pixel mapping. Opt Express 2005;13:9175–80.
[13] Shin D-H, Kim E-S. Computational integral imaging reconstruction of 3D object using a depth conversion technique. J. Opt. Soc. Korea 2008;12:131–5.
[14] Martínez-Corral M, Javidi B, Martínez-Cuenca R, Saavedra G. Multifacet structure of observed reconstructed integral images. J Opt Soc Am A 2005;22:597–603.
[15] Martínez-Cuenca R, Saavedra G, Pons A, Javidi B, Martínez-Corral M. Facet braiding: a fundamental problem in integral imaging. Opt Lett 2007;32:1078–1080.
[16] Blu T, Thevenaz P, Unser M. Linear interpolation revitalized. IEEE Trans Image Proc 2004;13:710–19.
[17] Keys RG. Cubic convolution interpolation for digital image processing. IEEE Trans Acoust Speech Signal Process 1981;29:1153–60.
[18] Shin D-H, -Yoo H. Image quality enhancement in 3D computational integral imaging by use of interpolation methods. Opt Express 2007;15:12039–12049.